LANGMUIR

Article

pubs.acs.org/Langmuir

Albumin (BSA) Adsorption over Graphene in Aqueous Environment: Influence of Orientation, Adsorption Protocol, and Solvent Treatment

J. G. Vilhena,[†,‡] Pamela Rubio-Pereda,[†,∥] Perceval Vellosillo,[†] P. A. Serena,[*,†] and Rubén Pérez[*,‡,§]

[†]Instituto de Ciencia de Materiales de Madrid (ICMM), CSIC, c/Sor Juana Ines de la Cruz 3, E-28049 Madrid, Spain

[‡]Departamento de Física Teórica de la Materia Condensada and [§]Condensed Matter Physics Center (IFIMAC), Universidad Autónoma de Madrid, E-28049 Madrid, Spain

[∥]Centro de Investigación Científica y de Educación Superior de Ensenada 3918, Postal Code 22860, Ensenada, Baja California, Mexico

ABSTRACT: We report 150 ns explicit solvent MD simulations of the adsorption on graphene of albumin (BSA) in two orientations and using two different adsorption protocols, i.e., free and forced adsorption. Our results show that free adsorption occurs with little structural rearrangements. Even taking adsorption to an extreme, by forcing it with a 5 nN downward force applied during the initial 20 ns, we show that along a particular orientation BSA is able to preserve the structural properties of the majority of its binding sites. Furthermore, in all the cases considered in this work, the ibuprofen binding site has shown a strong resilience to structural changes. Finally, we compare these results with implicit solvent simulations and find that the latter predicts an extreme protein unfolding upon adsorption. The origin of this discrepancy is attributed to a poor description of the water entropic forces at interfaces in the implicit solvent methods.

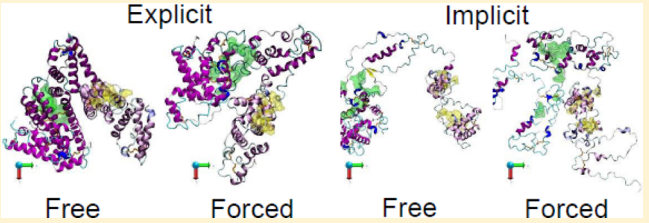

INTRODUCTION

The study of protein interaction with material surfaces is a subject of great fundamental and technological interest. From a technological point of view one finds a wide range of applications in biotechnology[1−4] and biomolecular engineering[1,5−7] which rely on protein adsorption. Among this broad spectra of applications one finds implant surfaces for improved biocompatibility,[2] biosensors,[7] and surfaces for tissue engineering and regenerative medicine.[3,6] One common feature to these applications is that the protein must remain bioactive. Given its importance, in the past decades, many experimental studies have tried to address this issue.[8] Nevertheless, due to their inherent limitations to probe events at an atomistic level, protein adsorption behavior on solid surfaces is still not well understood.[9] In the fundamental aspect, not only the mechanisms that drive the adsorption are ill understood[9−11] but they also play a crucial part on a manifold of biological interactions that occur inside live organisms.[8] Therefore, the understanding and control of protein adsorption on different surfaces remains a challenge of broad scientific and technological interest.

In the past years, graphene-based material arose as a promising material in biomedicine.[1,5,12−15] In particular, graphene's unique electrical and optical properties have led to a fruitful research in its use as an electrochemical and optical biosensor.[14] Furthermore, recent works[16] suggest that this material displays a key feature in implantology, such as biocompatibility, at least in selected applications for which it has been evaluated so far. This result arises from the biocompatibility observed in carbon-based materials[2,17] such as pyrolytic carbon,[17] commercially known as Pyrocarbon, and graphene sheets.[2] As a result, the manufacturing of long-term graphene-based medical implants and bioartificial sensors[14] has turned into another promising field of applications of this material. Nevertheless, success or failure of this kind of applications builds upon biological interactions at interfaces determined by blood plasma protein and substrate interactions.[1,5,8]

Accounting for about 60% of the total protein contained in blood plasma of mammalian systems,[18] serum albumins are among the first proteins to be adsorbed onto substrates inside biological systems.[19] As a result, albumins have been used for many years as model proteins to understand protein−substrate affinity.[20−22] This abundance inside mammal's plasma is related to the fact that they play a key role as carrier proteins[23] of a wide range of substances such as fatty acids, hormones, cations, and drugs such as phenylbutazone and ibuprofen. This enhances the interest in this particular protein since a small change in its structure not only might affect vital functions but also allow us to gain a deeper understanding of their stability

Received: August 24, 2015
Revised: January 22, 2016

DOI: 10.1021/acs.langmuir.5b03170
Langmuir XXXX, XXX, XXX−XXX

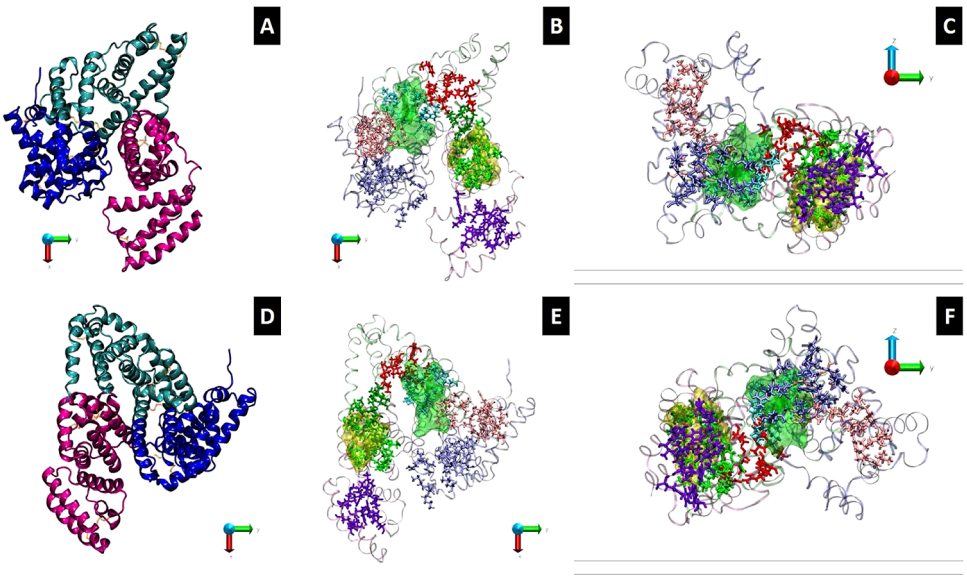

Figure 1. Top and side views of the pristine structure of the BSA molecule in orientation 1, top row, and orientation 2, bottom row. In the top views, the graphene substrate is not displayed for clarity. In (A) and (D), the secondary structure is colored according to domains: domain 1 in blue, domain 2 in cyan, and domain 3 magenta; disulfide bridges are shown in a bond representation colored in a light orange. In (B), (C), (E), and (F), the secondary structure colored by domain has been low-profiled while the FA1, FA2, FA3, FA4, FA5, FA6, and FA7 binding pockets—shown in a bond representation—are colored in pink, dark-green, bright-green, purple, red, and light-cyan, respectively; Sudlow sites 1 (2) are represented with a transparent green (yellow) Conolly surface.

and nonspecific interactions with surfaces. At last, it is important to mention that most of albumin studies are conducted on the bovine albumin[21] given its high degree of similarity with humans and its low cost and availability.

The comprehension of protein adsorption processes involved in biotechnological applications is essential to achieve materials with high biocompatibility and performance.[1,5,8−11,24] Nevertheless, protein adsorption over inorganic solid interfaces accounts for many molecular interactions. These kinds of interactions are difficult to analyze from experiments and are best revealed through atomistic computer simulations, such as molecular dynamics (MD). In fact, these kinds of simulations have turned into an essential tool to provide atomistic-level insights into protein−substrate interactions and validate experimental work in today's computational chemistry.[9,24]

Most of the theoretical studies concerning protein adsorption on graphene or other hydrophobic surfaces have focused on short peptide chains or small proteins like lysozyme and BMP-2. Among these works, the majority[24−30] observes a severe degree of unfolding, while a small minority[31−34] observes the opposite. The difference among these two classes of studies is that in the first case the solvent is treated using implicit solvent methods, while in the second set of works water is explicitly considered. Explicit solvent methods[35] should provide a more accurate description of the system, but the simulation times are limited by the large number of atoms resulting from the inclusion of water molecules. On the other hand, implicit solvent methods[36] involve approximations but allow a better exploration of the phase space. This open issue is still widely debated in the literature, with cases like lysozyme where earlier unfolding results coming from an implicit solvent study[26] have been questioned by more recent simulations using explicit water models.[32,34] Given the huge computational cost associated with describing the adsorption of a full-sized protein, to our knowledge, few works have considered the adsorption of such large protein over a surface.[37] In the paper by Mücksch et al.,[37] they simulate the adsorption of a full bovine serum albumin using implicit solvent methods, and they reach the conclusion that the protein loses almost completely its secondary structure upon adsorption to graphene. This result, together with simulations on the adsorption of albumin subdomains[25] also using implicit solvent methods, seems to lead to the conclusion that this material might not be biocompatible due to the apparent destruction of the most abundant plasma protein.

In this work, we used 150 ns explicit solvent molecular dynamics simulations to characterize the adsorption behavior of the BSA over bilayer graphene. The adsorption was conducted using two different protocols, i.e., free and forced adsorption (with a 5 nN downward force applied during the initial 20 ns). In both protocols, two initial BSA adsorption orientations were considered: one where BSA Sudlow sites are closer to the surface and another where these sites are far from it. By coupling the MD simulations with a thorough inspection of the BSA structural and functional properties, we are able to shed light on the interplay between adsorption and its functional and structural properties. In particular, we observed that free adsorption occurred with little structural rearrangements. Moreover, even in a more extreme adsorption scenario (forced), we realized that in a particular orientation, the BSA was able to preserve the structural properties of the majority of its binding sites. Furthermore, we also observed that the ibuprofen binding site showed a strong resilience to deformation. Finally, we have performed 15 ns implicit solvent MD simulations. In these simulations, we observed a extreme protein unfolding which is in contrast with the explicit solvent findings. The origin of this discrepancy is then attributed to a poor description of the water entropic forces at interfaces in the implicit solvent methods.

DOI: 10.1021/acs.langmuir.5b03170
Langmuir XXXX, XXX, XXX−XXX

SIMULATION METHODS

All simulations were performed using the AMBER software suite with NVIDIA GPU acceleration. In order to model the BSA and graphene, we used the force field ff12SB[38] and the OPLS aromatic carbon force field, present on AMBER generalized force field, respectively.[39] These force fields are known to properly describe biological systems[40] and accurately reproduce graphene mechanical and hydration properties.[41] Furthermore, the solvent was treated using two distinct methods, i.e., explicit and implicit solvation. For implicit solvation simulations, we used the generalized Born formalism with the OBC method[42] for the calculation of the Born radii. This model corrects some deficiencies[43,44] present in the original model of Hawkins, Cramer, and Truhlar[45] for the estimation of the effective radii for larger biomolecules. For explicit solvent simulations, the TIP3P water model[46] has been chosen. This water model suitably describes not only the interaction of water with proteins but also graphene's wetting properties.[24] We have used periodic boundary conditions with a orthorhombic unit cell that extends 20 Å above the protein in the direction normal to the surface. In order to solvate the system, this unit cell has been filled up with water molecules, placed in such a way that the minimum solute−water distance is 1 Å. The implicit solvent systems contain 29 136 atoms while the explicit solvent ones, including the water molecules, have a total of 269 904 atoms.

To perform the MD simulations, we resorted to the SHAKE algorithm[47] in order to use a 2 fs time step for integrating Newton's equation of motion. Atomic coordinates of the structures were stored every 2 ps. The particle mesh Ewald summation[48] was used to calculate long-range electrostatic interaction. The van der Waals interactions were truncated by applying a cutoff of 10 Å.

The X-ray crystallographic structure of BSA dimer was obtained from the protein data bank[49] with the PDB code 4f5s.[23] We then extracted the atomic coordinates of one BSA monomer and discarded the second BSA monomer as well as the poly(ethylene glycol) (PEG) ligand. Protons were added to the protein structure according to the calculated ionization states[50] of its titratable groups, at a blood pH of 7.4, characteristic of physiological conditions. The resulting structure had a net charge of −12 e, which was neutralized by adding 12 Na^+. Before the protein adsorption simulations, we have performed a 10 ns MD (both using implicit and explicit solvation) at 300 K and 1 atm to check the stability of this BSA structure. We observed a root-mean-square-deviation (RMSD) smaller than 2.5 Å, thus confirming its stability in both implicit and explicit solvent simulations, in agreement with a previous work.[37]

Following the initial protein structure preparation, BSA was geometrically centered above two 16 × 16 nm^2 AB stacked graphene layers along two different orientations (see Figure 1). In the initial configuration the protein's closest atom to the surface was at a distance of 10 Å from the first graphene layer. All graphene atoms are set to be neutral, and the bottom graphene layer was kept fixed. This setup mimics the typical configuration in many adsorption experiments where a graphene layer is supported on an inert, mechanically rigid substrate. In our case, the mechanical role of the solid substrate is simply described by the rigid graphene layer. We do not expect this choice to affect significantly to the adsorption properties, as the interaction between the bottom layer (that is as least 6 Å away from the BSA) is negligible compared with the interaction between the topmost graphene layer and the protein.

In all cases considered, BSA/graphene structures were energy minimized to avoid steric clashes using a combination of steepest descent and conjugate gradient methods. During this process, we kept weak restraints at the protein backbone and graphene substrate. Following the energy minimization stage, we thermalized the system during 1 ns on a NPT ensemble at a constant pressure of 1 atm and temperature of 300 K ensured by a Langevin thermostat.[51] Given the higher computational cost of a NPT simulation, and also that it is reasonable to assume that the system pressure should remain unaltered during the adsorption process, during the production runs (the ones following thermalization) we have kept the volume fixed by performing the simulations on a NVT ensemble.

BSA adsorption has been performed using two different protocols. The first consists in leaving the protein freely adsorb to the surface in a NVT ensemble during 150 ns. The second protocol is composed by two stages: initially we apply a constant downward force of 5 nN onto a selected group of atoms during 20 ns, and then by removing the force we leave the protein freely adsorb during 130 ns. In the case of implicit solvent simulations, to compensate for its ease in exploring the phase space, all the dynamics are 10 times shorter. Therefore, both free and forced adsorption only last 15 ns. In the forced adsorption protocol, the 5 nN force is applied on alpha carbons belonging to 16 cysteine residues evenly distributed over the protein. The disulfide bonds formed between cystine residues play an important role in the protein stability, and therefore by selecting this group of atoms, we ensure that no structural changes are induced when forces are applied.

Following the protein adsorption production runs the dynamics was analyzed by evaluating the following quantities: root-mean-square-deviation of BSA's backbone, domains, FA and DS sites;[52] the summation of radius of gyration components parallel to the surface;[52] the secondary structure as computed by the DSSP algorithm;[53,54] and the evolution of the contact surface. Among these quantities, the only one that requires further explanation is the computation of the adsorbed protein contact area. This quantity was computed resorting to Connolly's solvent-accessible surface area (SASA)[55] for the protein ($SASA_p$), for the graphene substrate ($SASA_g$), and the complex protein−substrate ($SASA_{pg}$). Then the contact area time evolution can be easily computed as $(SASA_p + SASA_g - SASA_{pg})/2$.

In order to compute desorption free energies for the two orientations considered in this work, we have have combined constant velocity steered molecular dynamics (SMD) simulations with the Jarzynski equality.[56] The SMD parameters that characterize the desorption process are the group of atoms to which the external force is applied, the spring constant of this force, and the velocity of the SMD. Our choices for these parameters are the following: the alpha carbons belonging to 16 cysteine residues evenly distributed over the BSA, a spring constant of 50 kcal/(mol Å), and a slow velocity of $\|v\| = 1$ Å/ns. As shown below, we have confirmed that this set of parameters fulfills two important requirements: It does not produce any structural rearrangement on the BSA, and it yields a stabilization (with null variation) of the desorption free energy[15] curve once the protein is far from the surface. For each orientation, the desorption free energy is obtained via the exponential average (i.e., using the Jarzynski equality[56]) of the

DOI: 10.1021/acs.langmuir.5b03170
Langmuir XXXX, XXX, XXX−XXX

work curves obtained in 10 independent SMDs with starting configurations sampled every 1 ns from the last 10 ns of simulation. The computation of the desorption free energy for two orientations has required additional 2(orientations) × 10(SMD repetitions) × 15(ns of simulation per SMD) = 300 ns of simulation.

Each MD/SMD simulation was performed using three nodes connected by Infiniband. Each node is composed by 12 Intel core processors at 2.53 GHz and 2 NVIDIA M2090 GPU accelerators (each with 512 CUDA cores and 6 GB of GDDR5 memory). Using this setup, our MD simulations ran at an average speed of 2.46 ns/day. Taking into consideration all the test and production runs for the adsorption simulations, and the desorption SMDs, these calculations consumed a total of 650.000 CPU hours.

RESULTS AND DISCUSSION

BSA Free Structural and Functional Properties. In order to shed light on the changes induced by the adsorption of the BSA to graphene, first we review some of BSA's structural properties. A first inspection of the structure (see Figure 1A) allows us to see that it is a heart-shaped globular protein. As all the other albumins, BSA is composed by three structurally similar domains, i.e., domain 1 (D1), domain 2 (D2), and domain 3 (D3), each represented with a different color in Figures 1A and 1D. Each of these three domains is composed by two subdomains, A and B, thus totaling six subdomains. The order of these subdomains is as follows: D1A-D1B-D2A-D2B-D3A-D3B, D1A being the subdomain A of domain 1, D1B the subdomain B of domain 1, D2A the subdomain A of domain 2, and so on. Concerning the BSA's secondary structure, the vast majority are α-helices (68%), followed by the turns/loops (10%). In each domain one finds ten helices that are distributed among two subdomains, i.e., subdomain A containing six helices and subdomain B containing four. These subdomains, i.e. A and B, are connected by a long flexible loop (see Figure 2, FA1 and FA5). In contrast with this, one finds that the division between domains 1 and 2 (the same goes for the division in domains 2 and 3) occurs in a very atypical fashion,[23] i.e., in the middle of a long α-helix. An example of this atypical division can be clearly seen in Figure 2, FA7, where we have a long α-helix that has two different colors corresponding to domains D1 (blue) and D2 (cyan), and Figure 2, DS2, with the α-helix divided between domains D2 (cyan) and D3 (magenta). Therefore, the conformational flexibility between those domains is governed by the helix bending, whereas the loop flexibility is responsible for the change in orientation between the subdomains. The stability inside each subdomain is assured by a network of disulfide bridges. In the subdomain A, the six helices are stabilized by four disulfide bridges, while in the subdomain B the four helices are stabilized by two disulfide bridges. Note that the subdomain 1A (D1A) is an exception since it only contains three bridges. It is noteworthy to stress that such is the importance of these bridges in holding the whole BSA structure together that their positions are preserved among all the known mammal albumins;[23] i.e., evolution seems to have kept them intact. Since all the above-mentioned properties affect the dynamics and flexibility of BSA, it is natural to assume that they shall guide the whole adsorption process of this protein to a surface.

To determine how the BSA's functional sites are affected and affect BSA's adsorption to graphene, it is of paramount importance to review some of BSA's functional properties here. Albumin works as a carrier protein in mammals bloodstream.[2] Therefore, during their evolution,[23] albumins have developed a large number of binding sites in order to bind to a broad spectrum of ligands with many different chemical properties. Among this large variety, here we focus solely on two functional groups, i.e., the seven fatty acid (FA) binding pockets and the two main sites dedicated to drug binding known as Sudlow sites (DS)[23] (see Figure 2). As shown in Figure 1, the seven FA pockets are evenly distributed over all the protein as follows: FA1 is in D1A and D1B, FA2 in D1A-B and D2A, FA3 in D2B and D3A, FA4 in D3A, FA5 in D3A and D3B, FA6 in D2A and D2B, and FA7 in D2A. As shown in Figure 2, most of the FA are distributed among two distinct subdomains. Given that subdomains are connected by long flexible loops (see e.g. FA1 and FA5 in Figure 2), this provides a mechanism for the pockets to change their volume and shape in order to bind to a given fatty acid. The amino acids in the Sudlow drug-binding sites DS1 and DS2 are located in D1A-D1B-D2A and D3A, respectively. Furthermore, as shown in Figures 1 and 2, DS1 contains part of the FA2 and FA7 pockets, while DS2 contains three of the residues of FA3 located in D3A and almost all residues of FA4. Given the nature of the binding affinity of the Sudlow sites, the changes induced by the adsorption are of great importance in the context of pharmaceutical applications, in particular to test the degree of resilience of each of these sites as well as its influence on the BSA adsorption to hydrophobic inorganic surfaces. Furthermore, given the high degree of similarity of the FA and DS sites between the BSA and HSA,[23] the conclusions derived from this work can be easily transposed to other albumins such as the human one.

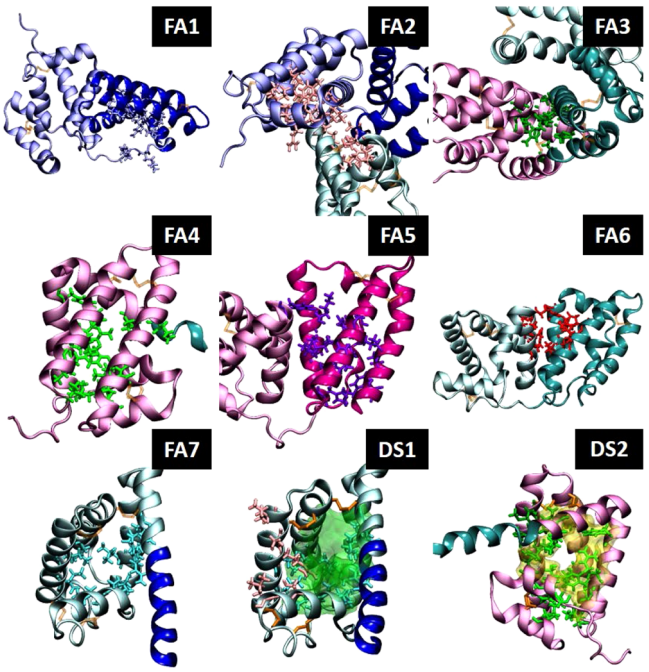

Figure 2. Seven fatty acid (FA) binding pockets and Sudlow sites 1 and 2 for drug binding. The representation is the same as the one used in Figure 1 with the sole difference that each domain is now colored using two different textures: metallic pastel for A subdomains and glossy for B subdomains.

BSA Free Adsorption: Structural Dynamics. Here we simulate the BSA adsorption over graphene along two distinct orientations that have been considered in previous studies.[37] In

DOI: 10.1021/acs.langmuir.5b03170
Langmuir XXXX, XXX, XXX−XXX

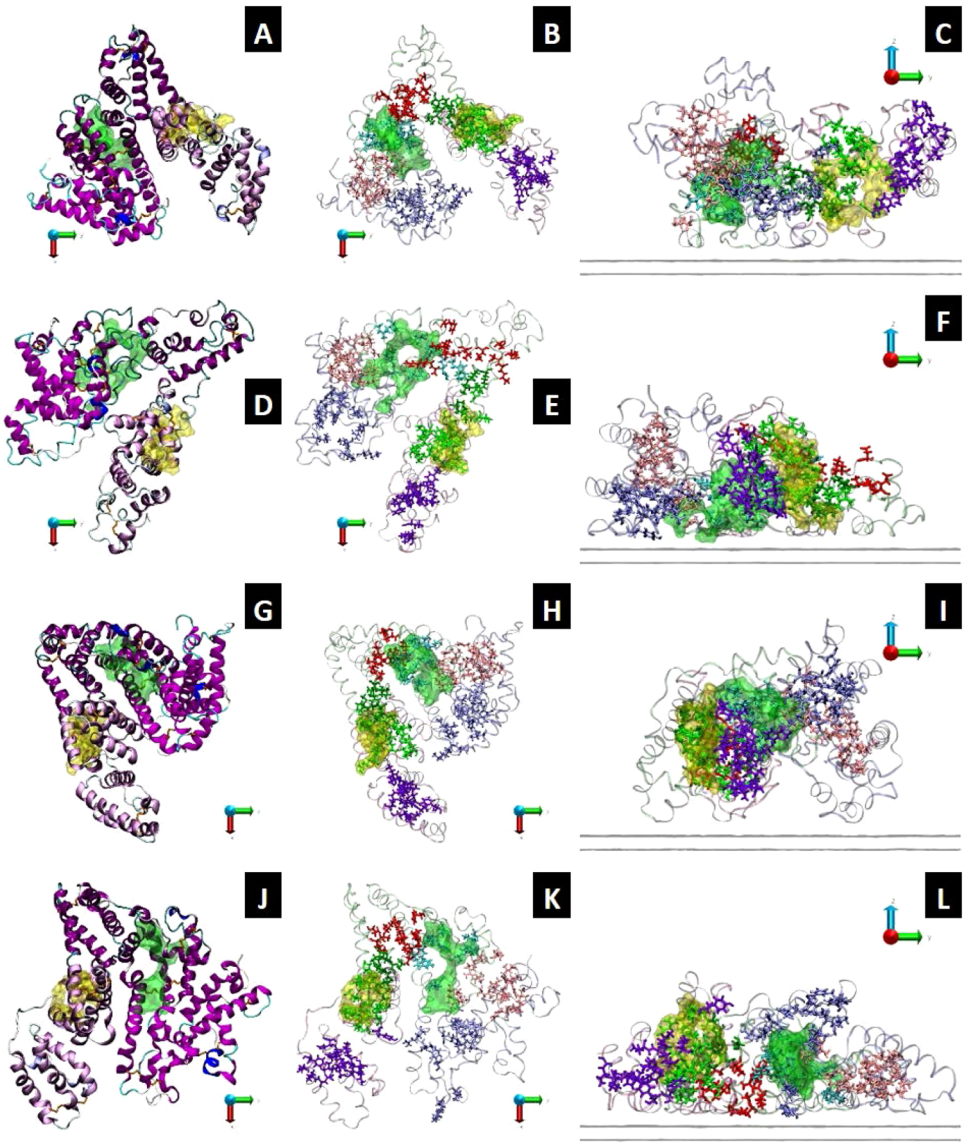

Figure 3. Top and side view snapshots of the final configurations of the BSA adsorbed along orientations 1 and 2 on the graphene substrate following two different protocols. In A-F/G-L the BSA is adsorbed in orientation 1/2 with a free-adsorption protocol (A-C and G-I) and a forced/free adsorption protocol (D-F and J-L). Secondary structure, FA binding pockets, and Sudlow sites are represented as in Figures 1 and 2.

the first row of Figure 1 we can observe the initial top (Figure 1A,B) and side (Figure 1C) views of the BSA in a orientation we shall call from here forth orientation 1 (O1). In the second row of Figure 1 we can observe analogous representation for a different orientation of BSA with respect to the surface. This last orientation will be referred to as orientation 2 (O2). The choice of these two orientations is motivated by the position of the DS sites. The O1 (see Figure 1C) not only allows us to bring the two sites as close as possible to the surface but also exposes the bottom part of these pockets to the surface. Since these pockets are mostly composed by hydrophobic residues, this particular configuration might enhance the BSA adsorption process. The second orientation positions the DS sites away from the surface, thus attempting to mitigate the role played by these sites during the adsorption process.

In Figure 3 we represent the final configurations of the free and forced adsorption of the BSA over graphene along two different orientations of adsorption. In all cases we observe that in these conditions, i.e. pH of 7.4 and desalinated water, the adsorption process is spontaneous. Furthermore, a close inspection of Figures 3A, 3D, 3G, and 3J allows us to see that the secondary structure is mostly preserved upon adsorption in all cases. In fact, the larger changes in the secondary structure are located at the protein−surface interface, where α-helix is transformed totally or partially in turns. At last, another common element is that the ibuprofen binding site, i.e. the DS2, seems to be structurally stable in all cases. Aside from these similarities, we can observe that O1 and O2 adsorb in a very distinct manner mainly due to the positioning of the Sudlow (DS) sites and the orientation of the intradomain long flexible loops.

In Figure 3A−C we show the top and side views of the BSA freely adsorbed to graphene along O1. Overall, we can observe that the structural changes are minimal as reflected by the low RMSD shown in Figure 4. The minor changes occurring in this structure are a result of the flexible elements of the BSA, i.e., the intradomain connections D2A-D2B and D3A-D3B. In fact, by comparing Figure 1A with Figure 3A, one realizes that in the

DOI: 10.1021/acs.langmuir.5b03170
Langmuir XXXX, XXX, XXX−XXX

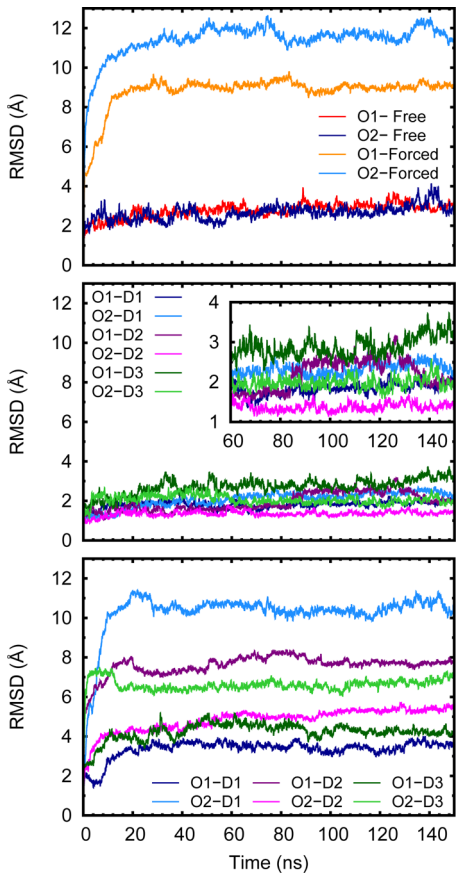

Figure 4. Root-mean-square-deviation (RMSD) for the backbone atoms (top row) and for the protein domains with a free (middle row) and forced adsorption protocol (bottom row).

adsorbed configuration the D3 moved apart from D1, thus opening a void in the middle of the protein. This occurs because of the long flexible loop connecting D2A-D2B that partially adsorbed to the surface acts as a hinge, thus allowing D3 to move slightly apart from D1 and consequently providing an extra mobility required to adsorb. A similar process occurs in the D3A-D3B, but with a more interesting origin. The site DS2 is located in D3A, which is strongly adsorbed. More interestingly, this adsorption is mediated by the bottom residues of DS2, which are mostly hydrophobic, thus leaving the pocket perpendicularly oriented with respect to the surface and still accessible from outside. In contrast with this behavior, we observe that D3B, in spite of being located in the same domain, oscillates back and forth with no special affinity with the surface. This movement, allowed by the long flexible loop D3A-D3B, can be clearly seen in the oscillatory nature of the RMSD of D3 shown in Figure 4. This result clearly shows that the strong adsorption occurring in this domain is mostly driven by the DS2 site. Concerning the DS1 site, as it can be seen in Figure 3C, we also observe that it moves closer to the surface partially deforming the secondary structure underneath. In this case, the adsorption of the site is not as pronounced as for the DS2, mostly because the residues of long flexible loop connecting D2A-D2B are blocking DS1 adsorption.

In Figure 3G–I we show the top and side views of the BSA freely adsorbed to graphene along orientation 2. Here again, both the secondary and tertiary structure are strongly preserved, and therefore the RMSD is very small (see Figure 4). Nevertheless, it is interesting to note that O2 adsorption occurs without any tilt of the protein nor with any major interdomain movement, which is contrast with O1 adsorption. The O2 adsorption occurs in three well-defined sites. The first being the α-helical residues in D1A located in the vicinity of the

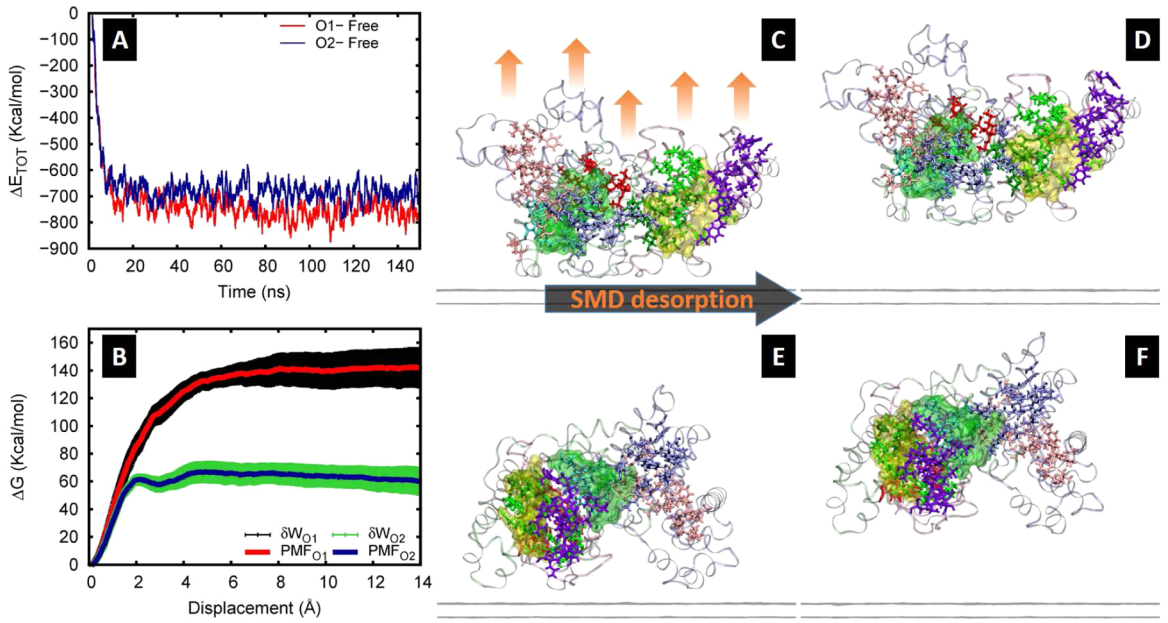

Figure 5. Desorption energies calculated from Steered MD simulations and the Jarzynski equality. (A) Time average (100 ps) of total energy change during the adsorption dynamics. The average of the total energy in the first 500 ps has been taken as our energy reference. (B) Free energy evolution along the desorption process averaged over 10 SMD simulations per orientation. We represent the maximum deviation δW for all SMD work curves (10 per orientation) with respect to the Jarzynski exponential averages. (C) Side view of the BSA adsorbed along orientation 1 after 145 ns MD simulation. (D) Side view of the BSA adsorbed along orientation 1 after one of the 10 SMD desorption simulations. (E) Side view of the BSA adsorbed along orientation 2 after 145 ns MD simulation. (F) Side view of the BSA adsorbed along orientation 2 after one of the 10 SMD desorption simulations. In (C–F), the secondary structure, FA binding pockets, and Sudlow sites are represented as in Figures 1 and 2.

DOI: 10.1021/acs.langmuir.5b03170
Langmuir XXXX, XXX, XXX–XXX

long flexible loop of this domain. This extra flexibility allows these helices to orient parallel to the surface. Nevertheless, this comes at a cost of partially losing their secondary structure. For this reason, we observe in Figure 4 that D1 has the largest contribution to the RMSD. The second adsorption site is located in a very small turn connecting the long interdomain (D2-D3) α-helix and a smaller helix of D2B. This adsorption site is particular rigid as can be appreciated by the lowest domain RMSD in Figure 4. The rigidity of this site not only is given by two S-bridges located in the vicinity of this turn but also is due to the structural rigidity provided by the very long α-helix. The third adsorption site of O2 is the long flexible loop connecting D3A-D3B. Despite being an extended region of adsorption, it barely affects BSA's secondary structure, mostly due to the high mobility associated with this site. In fact, in Figure 4 one can appreciate a small spike in RMSD. This spike occurs due to a small oscillatory movement occurring in the D3B. This subdomain being on one end free from the BSA and on the other attached to the surface by the long flexible domain is allowed to move freely on the aqueous solution. Concerning the DS sites, one observes that along this adsorption orientation they are not affected upon adsorption, as it was expected due to their initial distance to the surface.

The analysis presented so far confirms that the adsorption process does not affect the structural stability of the drug-binding sites DS1 and DS2. However, by comparing the structural dynamics of both orientations, we realize that these sites can play an important role in the adsorption to a hydrophobic surface. For O2, the DS sites are too far away to contribute significantly to the adsorption, whereas for O1, both DS sites are anchored to the surface by means of their hydrophobic residues located at the entry of these pockets. A preliminary quantification of this effect might be drawn from the time evolution of the total energy during the adsorption (see Figure 5A). From the average of the total energy in the last 70 ns of simulation for O1 (−753 kcal/mol) and for O2 (−691 kcal/mol), we can conclude that the proximity of the DS sites to the substrate in O2 seems to enhance the adsorption with an additional binding energy of 62 kcal/mol.

A proper estimation of the adsorption energy requires the evaluation of free energy differences between adsorbed and desorbed states that take into account the entropic forces not included in the total energy alone. We have computed the free energies of desorption (see Figure 5B) for both orientations with a combination of SMDs and the Jarzynski equality, as described in the Simulation Methods section. Figures 5C−F show that no spurious structural rearrangement has been induced in BSA during the desorption process, while Figure 5B confirms the stabilization (with null variation) of the desorption free energy[15] curves once the protein is far from the surface. Furthermore, the small maximum deviation of each SMD work curve to the Jarzynski free energy estimate (see δW in Figure 5B) supports that ten SMD repetitions per orientation are sufficient to determine the relative stability of the two orientations. The larger desorption free energy for O1 (141 kcal/mol) compared to O2 (63 kcal/mol) confirms the role of the hydrophobic residues in the DS sites in enhancing the adsorption of BSA to hydrophobic surfaces. The fact that the difference in free energies (74 kcal/mol) is larger than the change in the total energy during the adsorption (62 kcal/mol) highlights the role of entropic contributions in hydrophobic interactions.

BSA Forced Adsorption: Structural Dynamics. Now we focus on the BSA forced adsorption results. In this protocol, we apply a constant downward force of 5 nN during 20 ns in order to enhance the adsorption. To put this force value in context, current state-of-the-art atomic force microscopy is able to probe this class of biological samples with forces around 10 pN.[57,58] Therefore, here we are taking adsorption to extreme conditions which allow us to gain further insight into the resilience to mechanical deformations of BSA's structural and functional properties. From a first inspection of Figures 3 and 4 we can observe that the structural changes induced by the forced adsorption are more significant than the ones occurring in the free adsorption. In particular, in the forced adsorption protocol we observe (see Figures 3D and 3J) that DS1 is severely affected and that some secondary structure is lost upon adsorption, in contrast to the free adsorption results. In spite of these differences, it is surprising to observe that even under such extreme conditions some functional sites are barely affected, among these the most notable being the ibuprofen binding site DS2.

In Figures 3D−F we show the top and side views of the BSA forced adsorption to graphene along orientation 1. Comparing Figure 3A with Figure 3D, we observe that the forced adsorption protocol induces larger changes on the BSA structure, which are quantified in Figure 4. Furthermore, a careful inspection of these final configurations allows us to pinpoint the origin of these changes in two very specific sites, i.e., D3B and D2A.

The first difference between free and forced adsorption along O1 is located in D3B. While in the free protocol this subdomain is allowed to move freely in the solution, in the forced adsorption this subdomain is brought toward the surface, thus leading to its adsorption. As we can observe in Figure 4, this rearrangement of the subdomains D3A and D3B occurs very fast, and also from Figure 3D we can observe that it occurs without any massive loss of the secondary structure. This can be easily explained if we take into consideration that these subdomains are connected through a long flexible loop. While in the free adsorption protocol, this long flexible loop allowed D3B to move freely on solution, in the forced adsorption, this same loop provided the necessary mobility for D3B to tilt toward the surface without major resistance or loss of secondary structure.

The second site that contributes to a difference in the final adsorption configuration between the free and forced adsorption along O1 is mostly located in the subdomain D2A. In fact, from Figure 4, we can see that this domain is the one that presents the larger RMSD. When we force the adsorption, the long α-helix connecting D1B and D2A is brought toward the surface. While in D1 this helix is already close to the surface, in D2, this helix ends almost at the topmost part of the BSA. Therefore, by forcing the adsorption, one induces a downward movement of D2A, which in turn results into a deformation of this long α-helix so it orients parallel to the surface. This deformation is mostly accommodated by the topmost residues of the helix, i.e., the D2A residues. This process occurs with a greater cost than the one described in the D3B, and for this reason it takes longer to stabilize, as can be seen in the RMSD of D2 in Figure 4.

Concerning the DS sites, the major difference between the O1 free and forced adsorption is that DS1 initial tertiary structure is lost. Since DS1 is mostly located in D2A, it gets fully adsorbed over the surface. This leads to a spreading of this

DOI: 10.1021/acs.langmuir.5b03170
Langmuir XXXX, XXX, XXX−XXX

pocket over the surface, and therefore it is safe to assume that its functionality is lost, not only due to its inaccessibility but also due to the major structural changes induced by the adsorption. Concerning the DS2, overall we observe no major difference with respect to the free adsorption protocol. Nevertheless, it is interesting to observe that even though the forced adsorption tries to move the pocket parallel to the surface, it remains almost perpendicularly oriented as in the free adsorption protocol. Here again we observe that the large resilience of this pocket is mostly endowed by the strong S-bridges all around it.

In Figures 3J–L we show the top and side views of the BSA forced adsorption to graphene along orientation 2. During the dynamics, we observe that the major changes induced by the adsorption are focused on D3B and D1B-D2A.

In the O2 forced adsorption, in the D3B subdomain we observe that the long flexible loop, initially close to the surface, acts as a hinge point once adsorbed. As a result, not only D3A gets adsorbed but also D3B, that it is initially perpendicular to the surface but, after forcing the adsorption, is oriented parallel to it. This change is clearly reflected in the RMSD of D3 shown in Figure 4. Despite this drastic change in D3, in Figure 3J we can clearly distinguish three out of the initial four α-helices present on D3B domain. The one that is lost belongs to residues that are in direct contact with the surface. This highlights that despite the drastic change in the RMSD—mostly due to the flexible regions inside this subdomain—little secondary structure is lost.

The second most relevant change on the O2 forced adsorption occurs in subdomains D1B and D2A, D1B being the most affected. By forcing the adsorption, these regions are forced to move toward the surface, thus pushing D3 and D1A apart in order to reach the surface. This movement is allowed by two flexible loops: the one in D1 and the other on D2. As a result, little changes occur on the other subdomains, i.e., D1A, D3A, and D3B. Nevertheless, D1B, being the subdomain with the largest amount of residues on the topmost part of the BSA, is severely affected by this forced adsorption as shown in Figure 4. Furthermore, its interesting to note that the long α-helix connecting D1B and D2A keeps them together.

Overall, the O2 forced adsorption leads to the largest XY spreading of the BSA, as can be appreciated by comparing Figures 3B, 3E, 3H, and 3K. This could lead us to think that O2 is more prone to a forced unfolding due to the greater interaction area. However, from Figure 6, we realize that despite the unfolding induced by the forced adsorption, once we remove this force, BSA is able to partially recover its secondary structure. This is not the case for the O1 forced adsorption. Furthermore, the α-helical content of O2 is always larger. As the most fundamental difference between O1 and O2 is the proximity of the DS sites to the surface, this result seems to indicate that DS sites do play a relevant role in the adsorption process. A close inspection of DS2 reveals that the structure of this site is barely affected upon adsorption. In fact, comparing the free adsorption with the forced, i.e., Figures 3I and 3L, one realizes that even though DS1 is further apart from the surface in the free adsorption, in the forced protocol DS1 not only is closer to the surface than DS2 but also its structure has been severely affected by the adsorption, as can be seen in Figure 3K.

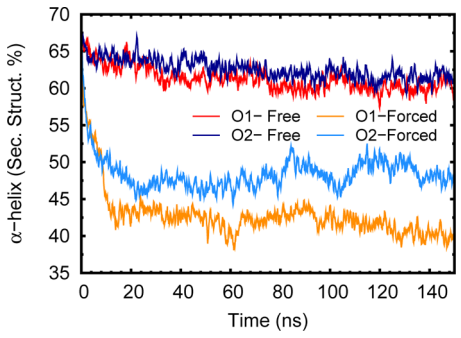

Figure 6. Time evolution of the secondary structure (α-helix) for the BSA adsorbed in both orientations (1 and 2) and with both protocols (free and forced).

Quantitative Comparison between Free and Forced Adsorption: Secondary Structure, Contact Area, and Protein Spreading. In order to give a more quantitative description of the BSA adsorption here, we will focus on the time evolution of the following quantities: α-helical content, contact area, and the radius of gyration parallel to the surface. Aside from the quantitative value, these observables allow us to have a general overview of the BSA adsorption process.

The most predominant secondary structure of BSA is the α-helix, constituting 68% of the total secondary structure. Therefore, analyzing its change allow us to understand to what degree the secondary structure, as well as BSA's functionality, are affected upon the different adsorption processes and orientations. In Figure 6, we represent the time evolution of the BSA α-helix for both orientations (O1 and O2) in both adsorption protocols (free and forced). As previously reported (see Figure 3), not only is the secondary structure of BSA barely affected upon adsorption but also the difference between O1 and O2 α-helix content is negligible. For these orientations the α-helical content stabilizes around 61% in the last 70 ns of simulation. Concerning the forced adsorption protocol, in Figure 6 we can observe that the content of α-helix for the O1 stabilizes around 40%, which is considerably smaller than one for the O2 (47%). Furthermore, in contrast with O1, O2 is able to partially recover from the secondary structure lost during the time we applied a force of 5 nN toward the surface (t < 20 ns). This recovery is mostly concentrated on the D3B. As for the relation between the contact area and the secondary structure, we observe that they are anticorrelated, i.e., a decrease in the secondary structure is coupled with an increase in the contact area (see Figures 6 and 7). In fact, most secondary structure lost during adsorption occurs at the protein–surface interface, where α-helices are converted into turns and random coils.

In Figures 7A–D, we represent the contact residues after free (A, C) and forced (B, D) BSA adsorption along orientations O1 and O2. From this figure we realize that there is no special preference for adsorbing hydrophobic/hydrophilic residues. Furthermore, the contact area of forced adsorption is significantly larger than the one obtained in the free adsorption protocol. This difference, about 18 nm^2, can be better appreciated in the time evolution of the contact area also shown in Figure 7.

In the bottom row of Figure 7, we represent the time evolution of the components of the radius of gyration (RoG) tensor parallel to the surface. This quantity allow us to measure the time evolution of the spreading of the BSA as it adsorbs along the four different cases considered. As qualitatively seen in Figure 3, here we observe that forced adsorption protocol

DOI: 10.1021/acs.langmuir.5b03170
Langmuir XXXX, XXX, XXX–XXX

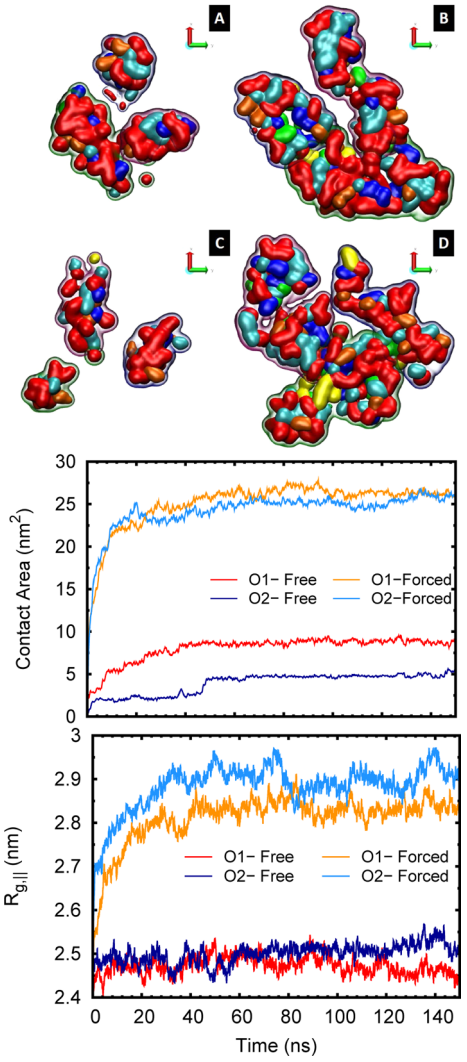

Figure 7. Top row: residue distribution for the BSA zone facing the graphene surface in a final configuration in both orientations; O1/O2 with a free (A/C) and forced (B/D) adsorption protocol. The residues color is in accordance with their hydrophobicity index:[59] very hydrophobic, hydrophobic, neutral, and hydrophilic residues are colored in blue, cyan, orange, and red, respectively. Yellow and green colored residues respectively correspond to hydrophilic and hydrophobic DS sites residues. Middle and bottom row show the time evolution of the contact surface area in nm^2 and the parallel component to the surface of the radius of gyration tensor for the BSA adsorbed in both orientations and with both protocols.

leads to a considerable increase of the protein spreading as compared to the free adsorption cases.

Changes on Fatty Acid and Sudlow Binding Sites upon Adsorption. In this section we recap the main changes induced on the FA and DS binding sites due to the BSA adsorption along the different orientations and protocols. In order to give a quantitative description of these changes, we will focus the analysis on the time evolution of the RMSD these sites. In order to put these values in context, it is important to stress that these are very flexible and mobile structures. In fact, in their native state in order to act as binding sites they need to change their volume.[23] Therefore, here we expect these sites to exhibit larger RMSD values than usual.

In the free adsorption protocol, we have previously observed that the RMSD of BSA's backbone is very small (Figure 4). The same happens to the RMSD of both the FA and DS binding sites, which remain always below 2.5 Å during the free adsorption along both orientations. Therefore, in free BSA adsorption, no matter the adsorption orientation (O1 or O2), the tertiary structure of the FA and DS sites is barely affected. As a result, the only *functional loss* would come from the inaccessibility of these sites once the protein is adsorbed.

In the forced adsorption protocol, we observe that under given circumstances the FA structure might be severely affected by the adsorption process. Inspecting the FA RMSD (see Figure 8) along forced O1 adsorption, we realize that only one out of the seven fatty acids remains with a RMSD below 3.5 Å. The structural changes observed in most pockets might have compromised the BSA bioactivity. In contrast with this behavior, for the O2, we observe that at least half of the FA binding pockets showed a RMSD below 3.5 Å. Furthermore, as shown in Figure 3, these sites are still accessible from the outside the protein; i.e., they are not buried between the BSA and the surface. Also in O2, we can observe that FA1 displays a strikingly large RMSD. This large mobility is associated with the fact that two FA1 residues are located in a long flexible loop (see Figure 2). As a result, they (an arginine and a leucine) are allowed to move freely, thus leading to this large RMSD. In fact, analyzing the dynamics of this pocket, we realize that the majority of its residues are kept intact during the adsorption; i.e., the large RMSD is coming from the detachment of these two residues. Nevertheless, these residues are essential for the FA1 site functionality,[23] since they work as gate keepers mediating the fatty acids to binding to FA1.[23] At last, by comparing O1 and O2 FA-RMSD (see Figure 8), we realize that along O1 adsorption the FA sites suffer considerably larger structural changes than the ones observed for the O2. Therefore, we expect that O2 adsorption is much more likely to preserve some FA-BSA bioactivity.

In the third column of Figure 8 we represent the RMSD of DS drug-binding sites in the forced adsorption protocol. Concerning their structural stability, two main conclusions can be drawn from Figure 8. The first being that as for the FA sites, the stability of the DS regions is more affected when BSA adsorbed along O1. The second is that in both O1 and O2 the ibuprofen binding site (DS2) systematically shows a higher resilience to deformation than the DS1 region. In fact, in the RMSD of DS2 forced O2 adsorption (bottom right graph in Figure 8), we observe that following the forced adsorption, DS2 is able to partially recover its initial tertiary structure. The resilience of the DS2 site is consistent with the fact that it is entirely located inside a subdomain. As a result, not only does it contain a smaller amount of mobile regions but also the surrounding sulfur bridges ensure a higher structural stability.

Comparison with Previous Works: Implicit Solvent. A molecular dynamics simulations of free and forced adsorption of the BSA on graphene was previously reported in the literature.[37] In that work,[37] the authors claim that upon (free and forced) adsorption BSA shows an extreme unfolding. Upon adsorption, Mucksch et al.[37] observed that BSA α-helical content is reduced to only 20%, out of a initial content of 68%. This extreme loss of secondary structure occurs due to a drastic change on the tertiary structure, since upon adsorption BSA is considerably spread over the surface. In contrast with these findings, here we have shown that the adsorption over graphene yields much milder changes on the BSA structural and functional properties. From a methodological point of view, our work differentiates from the work reported in ref 37 in

DOI: 10.1021/acs.langmuir.5b03170
Langmuir XXXX, XXX, XXX−XXX

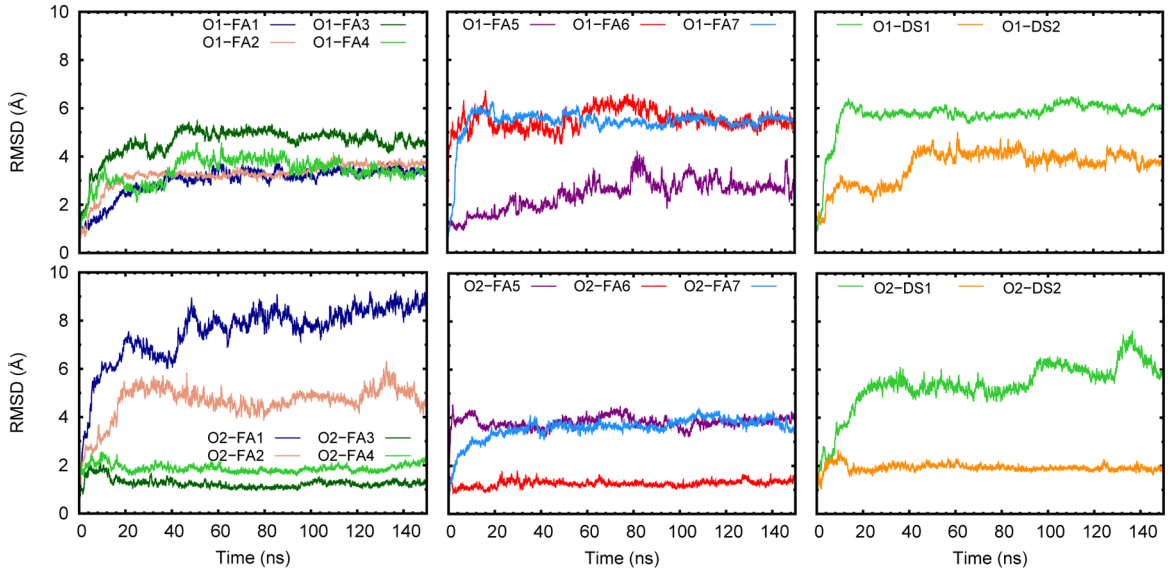

Figure 8. Time evolution of the RMSD for the atoms belonging to the FA binding pockets (left and middle column) and the Sudlow sites (right column) for the BSA forced adsorption protocol along in orientation 1 (top row) and 2 (bottom row).

three main aspects. The first difference is the initial atomic configuration of the BSA. In our work, the initial BSA structure was obtained from X-ray diffraction data, while in ref 37 BSA was built through homology modeling with HSA. The second main methodological difference is the simulation time. Here our MD simulations span 150 ns while in ref 37 the simulation time is of 20 ns. The third and last difference concerns the description of the solvent environment. Here we represent the solvent by explicitly including 80 256 water molecules (TIP3P model[46]), while in the work in ref 37, the solvent is described using an implicit solvation method. All the other aspects of the MD simulations (e.g., adsorption protocols, orientations, etc.) are similar in both works. In what follows, by isolating each of these differences, we tried to address the origin of such discrepancy.

To determine whether the difference arose from the different initial atomic configuration, we performed implicit solvent simulations using the same implicit solvation model as the one reported in ref 37 as well as similar simulation protocols, i.e., free and force (for further details see Simulation Methods section). The difference with respect to that work[37] is that now we use as the initial BSA structure the X-ray diffraction data.[23] Even though we repeated the simulation for the two orientations, and for each we applied both adsorption protocols (free and forced), here we discuss only on the results obtained for the orientation 1, since the conclusion drawn from it equally apply to O2. In Figures 9C,D we represent the top views of the final adsorption configuration obtained after the 15 ns of simulation with the implicit solvent method using the free adsorption protocol (Figure 9C) and the forced adsorption protocol (Figure 9D). These results agree with the ones in ref 37: BSA shows a considerable spreading over the surface. Furthermore, also the α-helix content of the adsorbed BSA is very similar to the one reported in ref 37. For the forced adsorption here we find that the α-helical content after the adsorption is of 19%, while in ref 37 it is of 17.8%. These results clearly discard the possibility that the difference between our explicit solvent simulations and the ones in the ref 37 could come from the different initial coordinates used.

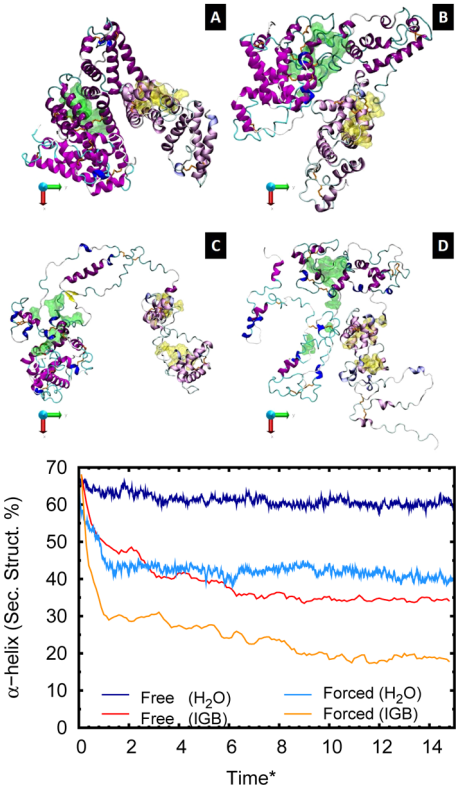

Figure 9. From (A) to (D), top views of the final configurations of the BSA in orientation 1 with explicit/implicit solvent (AB/CD) and with a free/forced adsorption protocol (AC/BD). Time evolution of the secondary structure (α-helix) for the BSA molecule adsorbed in orientation 1 with implicit/explicit solvent and with free/forced adsorption protocols.

From our implicit solvent simulations we realize that the difference between our (explicit solvent) results and the BSA adsorption reported in ref 37 could only come from either the solvation method or the simulation time. In fact, these two quantities are tightly coupled. In explicit solvent simulations, the presence of water molecules causes substantial frictional

DOI: 10.1021/acs.langmuir.5b03170
Langmuir XXXX, XXX, XXX−XXX

drag on the protein and viscous effects that are not present in implicit solvent simulations. As a result, the kinetics of conformational movement is much accelerated in implicit solvent simulations. Therefore, a fair comparison between explicit solvent and implicit solvent simulations requires that the former has much larger simulation times in order to achieve an equivalent exploration of the configuration space in both cases. To compensate for this difference, our explicit solvent simulations lasts 150 ns, i.e., 10 times longer than the implicit solvent MDs. When we compare the results obtained in each of these solvation methods, we realize that, in contrast with explicit solvent results (see Figures 9A,B), implicit solvent simulations (see Figures 9A,B) exhibit an extreme degree of unfolding. Even considering only forced adsorption explicit solvent results, the unfolding induced in this case is smaller than the one obtained using implicit solvent free adsorption simulations. This difference can be better appreciated by analyzing the evolution of the main secondary structure component (α-helix) of the BSA in each case (see Figure 9E). Taking into account that neither forced adsorption nor a 10 times longer explicit solvent simulation lead to the same degree of unfolding obtained in implicit solvent simulations, we are led to conclude that implicit solvation is misrepresenting key interactions and therefore not correctly describing the adsorption of the BSA over graphene.

The larger computational cost of explicit solvent simulations, from both the number of atoms and the larger simulation times, comes with an important advantage: a more accurate description of the solvent and its entropic properties. In implicit solvent MD simulations, the behavior of solvent molecules is approximated by an effective mean-field potential with the following general form:[42]

$$\Delta G_{solv} = \Delta G_{el} + \Delta G_{nonel} \quad (1)$$

where ΔG_{el} accounts for the change in the electrostatic interaction between the molecule atoms due to the presence of a continuum solvent (dielectric) and ΔG_{nonel} comes from a combination of two effects: the unfavorable cost of disrupting the water H-bound network around the solute and the favorable van der Waals attraction between solute and solvent. Therefore, the second term includes all the water entropic effects. Furthermore, the vast majority of implicit solvent methods used to simulate this kind of systems[60−64] have the following form:

$$\Delta G_{nonel} = \gamma SA \quad (2)$$

where SA is total solvent accessible surface area of the molecule and γ is a positive proportionality constant derived from experimental solvation energies of small nonpolar molecules. Taking into consideration that hydrophobic forces, i.e., water entropy forces, are one of the most important forces driving protein adsorption,[8] one realizes that such coarse approximation to water entropic forces taken in implicit solvent models might drastically affect the final adsorption configuration.

When a protein is approaching a surface, the solvent accessible area of the system surface + protein suffers a sudden reduction on the SA (on the order to the total protein SA). As a result ΔG_{nonel} ($= G_{nonel}^{adsorbed} - G_{nonel}^{free} < 0$) suddenly peaks on negative values, thus leading to strong hydrophobic adsorption force. This abrupt change on the SA does not happen in most of implicit solvent applications where one is usually focused on single molecules or at most interaction of a small ligand to a protein.[8] In summary, large differences between implicit models with experiments or explicit solvent approaches are generally expected when the properties of water molecules are substantially different from the bulk solvent, such as the case of media interfaces. Despite the fact that a true validation of one of these two approaches (implicit solvation or explicit solvation) can only be brought through high-resolution experiments such as frequency-modulation AFM, caution is advised when using implicit solvent methods to describe protein adsorption.

Limitations of Simulation Methods. The results presented so far clearly show that MD simulations are a powerful tool to explore protein−substrate interactions. However, in the absence of experiments, it is necessary to be particularly critical in the assessment of the possible limitations of this theoretical approach. Our simulations, as the vast majority of theoretical works concerning protein adsorption,[24−30,32−34] are based on two main assumptions: the transferability of the force fields and the convergence of the MD simulations.

The first assumption is that the force fields employed in this study, OPLS for graphene and AMBER-FF12SB for the protein in solution, are able to accurately describe the interactions between the amino acid residues and the surface. This common assumption is obviously a major concern and is backed by a number of combined experimental and theoretical studies where a detailed comparison has been made on a model system—the work of Horinek et al.[31] in one of these examples. They compared MD simulation results and atomic force microscopy experiments for the adsorption of small peptides on hydrogen-terminated or hydroxyl-terminated diamond surfaces and concluded that standard force fields (GROMOS96[65]) are capable of resolving the fine details of the hydrophobic peptide−surface interaction. Based on these results, it is natural to expect that more developed and sophisticated potentials, as those used in our simulations, should be able to describe properly the interaction of a whole protein with another carbon-like substrate. However, as stated above, a final confirmation of the force field transferability, i.e., the suitability of OPLS+AMBER-FF12S to reproduce the graphene−peptide interactions, awaits experimental validation, and we hope that our results will stimulate future work along this line.

The second assumption is that the MD simulations are long enough for the system to reach a thermal equilibrium state. It is extremely difficult, if not impossible, to determine, from a theoretical study alone, if a MD simulation has reached an actual equilibrium configuration. Given the complexity and size of the BSA, it may well be that after 150 ns (already a long simulation in terms of the computational resources needed to study the adsorption of a protein of this size) the system is still locked in a metastable state, thus resulting in apparently converged observables. New hardware advances and algorithmic developments are continuously pushing the limit toward longer simulation times. Accelerated sampling methods might provide an additional confirmation since they are able to sample the conformational phase space more efficiently than conventional MD simulations. Nevertheless, as in the case of the transferability, the ultimate proof of having reached an actual thermal equilibrium state in either conventional or accelerated MD simulations can only be provided through experiments.

The limitations here exposed emphasize the need for additional experimental studies to quantitatively characterize

DOI: 10.1021/acs.langmuir.5b03170
Langmuir XXXX, XXX, XXX−XXX

the behavior of this kind of complex molecular systems. In fact, when describing protein adsorption processes, MD simulations and experiments form a perfect synergy. On the one hand, simulations are able to provide information at an atomic level as well as unraveling the role played by the many different interactions, issues that are not accessible to experiments. On the other hand, experiments are able to provide information on complex systems working in actual conditions, discovering new phenomenology and validating in some controlled conditions the simulations.

CONCLUSIONS

In this work, we used 150 ns explicit solvent molecular dynamics simulations to characterize the adsorption behavior of the BSA over a bilayer graphene surface. The adsorption was conducted using two different protocols, i.e., free and forced adsorption (with a 5 nN downward force applied during the initial 20 ns). In both protocols, two initial BSA adsorption orientations were considered: the O1 where FA and DS sites are closer to the surface and O2 where FA and DS sites are far from it.

In the free adsorption protocol, the structural (tertiary and secondary) changes induced by the adsorption were minimal in both orientations. In the forced adsorption protocol, the changes induced by the adsorption were considerably larger. Nevertheless, since most of the changes are located at the protein surface interface, the O2 preserved most of the structural properties of FA and DS binding sites, while O1 suffered the largest structural changes on the FA/DS binding sites. It is remarkable that even under such extreme conditions O2 was able to preserve the structural properties of the majority of FA and DS sites. Therefore, we think that for graphene based biosensing devices the O2 orientation would be the most favorable.

Concerning the binding sites, in all the cases considered here, we observed a strong structural resilience of the ibuprofen binding site (DS2). Taking into consideration its location and resilience to structural deformations, we expect that after adsorption this site will still remain bioactive; i.e., it will preserve its ability to trap the ibuprofen molecule. Its strong resilience has a twofold origin. Unlike most of BSA binding sites, DS2 lacks residues located in mobile regions, since it is mostly located in α-helix structures. Also, the presence of a very strong network of disulfide bridges located around this pocket makes it endure large mechanical deformations.

We have compared explicit solvent adsorption results with implicit solvent simulations and found a large discrepancy between both methods. While in the 150 ns explicit solvent simulation we observed that BSA structure is mostly preserved upon adsorption, 15 ns implicit solvent models predict a severe protein unfolding. We believe that the reason for such discrepancy arises from a poor description of the hydrophobic forces in implicit solvent simulations of protein adsorption, a situation where drastic changes in the solvent−protein contact area take place and the entropic behavior of water molecules is very different from bulk solution properties (the framework under which those models were developed).

Finally, we hope that our findings regarding the preservation of the BSA structure upon adsorption and, in particular, the resilience of some of the binding sites relevant for its biological activity, will promote new experimental studies on the adsorption of proteins on graphene and other carbon nanostructures. These experiments are crucial to confirm our theoretical predictions, to promote possible applications, and to further validate the simulation protocols used in this field.

AUTHOR INFORMATION

Corresponding Authors

*E-mail: pedro.serena@icmm.csic.es (P.A.S.).
*E-mail: ruben.perez@uam.es (R.P.).

Notes

The authors declare no competing financial interest.

ACKNOWLEDGMENTS

We acknowledge the financial support from the Spanish MINECO (projects Consolider Force-For-Future CSD2010-00024, MAT2011-023627, MAT2012-2448, FIS2012-36113-C03-03, MAT2013-44858-R, and MAT2014-54484-P) and Comunidad de Madrid (S2009/MAT-1467), and also the computer resources, technical expertise, and assistance provided by the Red Española de Supercomputación at the Minotauro Supercomputer (BSC, Barcelona) and the Extremadura Research Centre for Advanced Technologies (CETA-CIEMAT).

REFERENCES

(1) Oliveira, S. F.; Bisker, G.; Bakh, N. A.; Gibbs, S. L.; Landry, M. P.; Strano, M. S. Protein functionalized carbon nanomaterials for biomedical applications. *Carbon* **2015**, *95*, 767−779.
(2) Liu, H.; Webster, T. J. Nanomedicine for Implants: a Review of Studies and Necessary Experimental Tools. *Biomaterials* **2007**, *28*, 354−369.
(3) Zhang, Z.; Zhang, M.; Chen, S.; Horbett, T. A.; Ratner, B. D.; Jiang, S. Blood Compatibility of Surfaces With Superlow Protein Adsorption. *Biomaterials* **2008**, *29*, 4285−4291.
(4) Tamayo, J.; Kosaka, P. M.; Ruz, J. J.; Paulo, A. S.; Calleja, M. Biosensors Based on Nanomechanical Systems. *Chem. Soc. Rev.* **2013**, *42*, 1287−1311.
(5) De Leo, F.; Magistrato, A.; Bonifazi, D. Interfacing proteins with graphitic nanomaterials: from spontaneous attraction to tailored assemblies. *Chem. Soc. Rev.* **2015**, *44*, 6916−6953.
(6) Sanhai, W. R.; Sakamoto, J. H.; Canady, R.; Ferrari, M. Seven Challenges for Nanomedicine. *Nat. Nanotechnol.* **2008**, *3*, 242−244.
(7) Yanik, A. A.; Huang, M.; Kamohara, O.; Artar, A.; Geisbert, T. W.; Connor, J. H.; Altug, H. An Optofluidic Nanoplasmonic Biosensor for Direct Detection of Live Viruses from Biological Media. *Nano Lett.* **2010**, *10*, 4962−4969.
(8) Norde, W.; Horbett, T. A.; Brash, J. L. *Proteins at Interfaces III State of the Art*; ACS Symposium Series; American Chemical Society: 2012; Vol. *1120*, pp 1−34.
(9) Zhang, G. *Computational Bioengineering*; CRC Press: 2015; pp 293−326.
(10) Calvaresi, M.; Zerbetto, F. The Devil and Holy Water: Protein and Carbon Nanotube Hybrids. *Acc. Chem. Res.* **2013**, *46*, 2454−2463.
(11) Marchesan, S.; Prato, M. Under the lens: carbon nanotube and protein interaction at the nanoscale. *Chem. Commun.* **2015**, *51*, 4347−4359.
(12) Chen, G. Y.; Pang, D. W.-P.; Hwang, S.-M.; Tuan, H.-Y.; Hu, Y.-C. A Graphene-based Platform for Induced Pluripotent Stem Cells Culture and Differentiation. *Biomaterials* **2012**, *33*, 418−427.
(13) Markovic, Z. M.; Harhaji-Trajkovic, L. M.; Todorovic-Markovic, B. M.; Kepic, D. P.; Arsikin, K. M.; Jovanovic, S. P.; Pantovic, A. C.; Dramicanin, M. D.; Trajkovic, V. S. In Vitro Comparison of the Photothermal Anticancer Activity of Graphene Nanoparticles and Carbon Nanotubes. *Biomaterials* **2011**, *32*, 1121−1129.
(14) Zhen, L.; Mengyuan, H.; Dangdang, X.; Zhihong, L. Graphene Materials-Based Energy Acceptor Systems and Sensors. *J. Photochem. Photobiol., C* **2014**, *18*, 1−17.

DOI: 10.1021/acs.langmuir.5b03170
Langmuir XXXX, XXX, XXX−XXX

(15) Zhang, Y.; Nayak, T. R.; Hong, H.; Cai, W. Graphene: a Versatile Nanoplatform for Biomedical Applications. *Nanoscale* **2012**, *4*, 3833−3842.
(16) Shen, H.; Zhang, L.; Liu, M.; Zhang, Z. Biomedical Applications of Graphene. *Theranostics* **2012**, *2*, 283−294.
(17) Allieu, Y.; Winter, M.; Pequignot, J. P.; de Mourgues, P. Radial Head Replacement With a Pyrocarbon Head Prosthesis: Preliminary Results of a Multicentric Prospective Study. *Eur. J. Orthop. Surg. Tr.* **2006**, *16*, 1−9.
(18) Carter, D.; Ho, J. X. *Advances in Protein Chemistry*; Academic Press: New York, 1994; Vol. *45*, pp 153−203.
(19) Roy, R. K.; Lee, K. L. Biomedical Applications of Diamond-Like Carbon Coatings: A Review. *J. Biomed. Mater. Res., Part B* **2007**, *83B*, 72−84.
(20) Wertz, C. F.; Santore, M. M. Effect of Surface Hydrophobicity on Adsorption and Relaxation Kinetics of Albumin and Fibrinogen: Single-Species and Competitive Behavior. *Langmuir* **2001**, *17*, 3006−3016.
(21) Gelamo, E. L.; Silva, C. H. T. P.; Imasato, H.; Tabak, M. Interaction of Bovine (BSA) and Human (HSA) Serum Albumins With Ionic Surfactants: Spectroscopy and Modelling. *Biochim. Biophys. Acta, Protein Struct. Mol. Enzymol.* **2002**, *1594*, 84−99.
(22) Langdon, B.; Kastantin, M.; Schwartz, D. Apparent Activation Energies Associated with Protein Dynamics on Hydrophobic and Hydrophilic Surfaces. *Biophys. J.* **2012**, *102*, 2625−2633.
(23) Bujacz, A. Structures of Bovine, Equine and Leporine Serum Albumin. *Acta Crystallogr., Sect. D: Biol. Crystallogr.* **2012**, *68*, 1278−1289.
(24) Raffaini, G.; Ganazzoli, F. Understanding the Performance of Biomaterials through Molecular Modeling: Crossing the Bridge between their Intrinsic Properties and the Surface Adsorption of Proteins. *Macromol. Biosci.* **2007**, *7*, 552−566.
(25) Raffaini, G.; Ganazzoli, F. Surface Topography Effects in Protein Adsorption on Nanostructured Carbon Allotropes. *Langmuir* **2013**, *29*, 4883−4893.
(26) Raffaini, G.; Ganazzoli, F. Protein Adsorption on a Hydrophobic Surface: A Molecular Dynamic s Study of Lysozyme on Graphite. *Langmuir* **2010**, *26*, 5679−5689.
(27) Ganazzoli, F.; Raffaini, G. Computer Simulation of Polypeptide Adsorption on Model Biomaterials. *Phys. Chem. Chem. Phys.* **2005**, *7*, 3651−3663.
(28) Raffaini, G.; Ganazzoli, F. Simulation Study of the Interaction of Some Albumin Subdomains With a Flat Graphite Surface. *Langmuir* **2003**, *19*, 3403−3412.
(29) Mücksch, C.; Urbassek, H. M. Adsorption of BMP-2 on a Hydrophobic Graphite Surface: A Molecular Dynamics Study. *Chem. Phys. Lett.* **2011**, *510*, 252−256.
(30) Mücksch, C.; Urbassek, H. M. Enhancing Protein Adsorption Simulations by Using Accelerated Molecular Dynamics. *PLoS One* **2013**, *8*, e64883.
(31) Horinek, D.; Serr, A.; Geisler, M.; Pirzer, T.; Slotta, U.; Lud, S. Q.; Garrido, J. A.; Scheibel, T.; Hugel, T.; Netz, R. R. Peptide adsorption on a hydrophobic surface results from an interplay of solvation, surface, and intrapeptide forces. *Proc. Natl. Acad. Sci. U. S. A.* **2008**, *105*, 2842−2847.
(32) Wei, T.; Carignano, M. A.; Szleifer, I. Lysozyme Adsorption on Polyethylene Surfaces: Why Are Long Simulations Needed? *Langmuir* **2011**, *27*, 12074−12081.
(33) Ou, L.; Luo, Y.; Wei, G. Atomic-Level Study of Adsorption, Conformational Change, and Dimerization of an α-Helical Peptide at Graphene Surface. *J. Phys. Chem. B* **2011**, *115*, 9813−9822.
(34) Wei, T.; Carignano, M. A.; Szleifer, I. Molecular Dynamics Simulation of Lysozyme Adsorption/Desorption on Hydrophobic Surfaces. *J. Phys. Chem. B* **2012**, *116*, 10189−10194.
(35) Bizzarri, A. R.; Cannistraro, S. Molecular Dynamics of Water at the Protein-Solvent Interface. *J. Phys. Chem. B* **2002**, *106*, 6617−6633.
(36) Feig, M.; Brooks, C. L. Recent Advances in the Developments and Application of Implicit Solvent Models in Biomolecule Simulations. *Curr. Opin. Struct. Biol.* **2004**, *14*, 217−224.
(37) Mücksch, C.; Urbassek, H. M. Molecular Dynamics Simulation of Free and Forced BSA Adsorption on a Hydrophobic Graphite Surface. *Langmuir* **2011**, *27*, 12938−12943.
(38) AMBER12. 2012; http://ambermd.org/.
(39) Wang, J.; Wolf, R. M.; Caldwell, J. W.; Kollman, P. A.; Case, D. A. Development and Testing of a General Amber Force Field. *J. Comput. Chem.* **2004**, *25*, 1157−1174.
(40) Brandt, J. P.; Patapoff, T. W.; Aragon, S. R. Construction, MD Simulation, and Hydrodynamic Validation of an All-Atom Model of a Monoclonal IgG Antibody. *Biophys. J.* **2010**, *99*, 905−913.
(41) Tsai, J.-L.; Tu, J.-F. Characterizing Mechanical Properties of Graphite Using Molecular Dynamics Simulation. *Mater. Eng.* **2010**, *31*, 194−199.
(42) Onufriev, A.; Bashford, D.; Case, D. A. Exploring Protein Native States and Large-Scale Conformational Changes With a Modified Generalized Born Model. *Proteins: Struct., Funct., Genet.* **2004**, *55*, 383−394.
(43) Grycuk, T. Deficiency of the Coulomb-field Approximation in the Generalized Born Model: An Improved Formula for Born-radii Evaluation. *J. Chem. Phys.* **2003**, *119*, 4817−4826.
(44) Bashford, D.; Case, D. A. Generalized Born Models of Macromolecular Solvation Effects. *Annu. Rev. Phys. Chem.* **2000**, *51*, 129−152.
(45) Hawkins, G. D.; Cramer, C. J.; Truhlar, D. G. Parametrized Models of Aqueous Free Energies of Solvation Based on Pairwise Descreening of Solute Atomic Charges from a Dielectric Medium. *J. Phys. Chem.* **1996**, *100*, 19824−19839.
(46) Jorgensen, W. L.; Chandrasekhar, J.; Madura, J. D.; Impey, R. W.; Klein, M. L. Comparison of Simple Potential Functions for Simulating Liquid Water. *J. Chem. Phys.* **1983**, *79*, 926−935.
(47) Ryckaert, J. P.; Ciccoti, G.; Berendsen, H. J. C. Numerical Integration of the Cartesian Equation of Motion of a System With Constraints: Molecular Dynamics Calculations. *J. Comput. Phys.* **1977**, *52*, 24−34.
(48) Darden, T.; York, D.; Pedersen, L. Particle Mesh Ewald: an N-log(N) Method for Ewald Sums in Large Systems. *J. Chem. Phys.* **1993**, *98*, 10089−10092.
(49) Berman, H. M.; Westbrook, J.; Feng, Z.; Gilliland, G.; Bhat, T. N.; Weissig, H.; Shindyalov, I. N.; Bourne, P. E. The Protein Data Bank. *Nucleic Acids Res.* **2000**, *28*, 235−242.
(50) Gordon, J. C.; Myers, J. B.; Folta, T.; Shoja, V.; Heath, L. S.; Onufriev, A. H++: a Server for Estimating pKas and Adding Missing Hydrogens to Macromolecules. *Nucleic Acids Res.* **2005**, *33*, W368−W371.
(51) Loncharich, R. J.; Brooks, B. R.; Pastor, R. W. Langevin Dynamics of Peptides: The Frictional Dependence of Isomerization Rates of N-acetylalanyl-N'-methylamide. *Biopolymers* **1992**, *32*, 523−535.
(52) Roe, D. R.; Cheatham, T. E. PTRAJ and CPPTRAJ: Software for Processing and Analysis of Molecular Dynamics Trajectory Data. *J. Chem. Theory Comput.* **2013**, *9*, 3084−3095.
(53) Joosten, R. P.; te Beek, T. A. H.; Krieger, E.; Hekkelman, M. L.; Hooft, R. W. W.; Schneider, R.; Sander, C.; Vriend, G. A series of PDB related databases for everyday needs. *Nucleic Acids Res.* **2011**, *39*, D411.
(54) Kabsch, W.; Sander, C. Dictionary of Protein Secondary Structure: Pattern Recognition of Hydrogen-Bonded and Geometrical Features. *Biopolymers* **1983**, *22*, 2577−2637.
(55) Connolly, M. L. Analytical Molecular Surface Calculation. *J. Appl. Crystallogr.* **1983**, *16*, 548−558.
(56) Jarzynski, C. Nonequilibrium Equality for Free Energy Differences. *Phys. Rev. Lett.* **1997**, *78*, 2690−2693.
(57) Noy, A.; Friddle, R. W. Practical Single Molecule Force Spectroscopy: How to Determine Fundamental Thermodynamic Parameters of Intermolecular Bonds With an Atomic Force Microscope. *Methods* **2013**, *60*, 142−150.
(58) Hutter, J. L.; Bechhoefer, J. Calibration of Atomic Force Microscope Tips. *Rev. Sci. Instrum.* **1993**, *64*, 1868−1873.

DOI: 10.1021/acs.langmuir.5b03170
Langmuir XXXX, XXX, XXX−XXX

(59) Monera, O. D.; Sereda, T. J.; Zhou, N. E.; Kay, C. M.; Hodges, R. S. Relationship of Sidechain Hydrophobicity and α-Helical Propensity on the Stability of the Single-Stranded Amphipathic α-Helix. *J. Pept. Sci.* **1995**, *1*, 319−329.
(60) Hawkins, G. D.; Cramer, C. J.; Truhlar, D. G. Parametrized Models of Aqueous Free Energies of Solvation Based on Pairwise Descreening of Solute Atomic Charges From a Dielectric Medium. *J. Phys. Chem.* **1996**, *100*, 19824−19839.
(61) Onufriev, A.; Bashford, D.; Case, D. A. Modification of the Generalized Born Model Suitable for Macromolecules. *J. Phys. Chem. B* **2000**, *104*, 3712−3720.
(62) Onufriev, A.; Bashford, D.; Case, D. A. Exploring Protein Native States and Large-Scale Conformational Changes With a Modified Generalized Born Model. *Proteins: Struct., Funct., Genet.* **2004**, *55*, 383−394.
(63) Feig, M.; Onufriev, A.; Lee, M.; Im, W.; Case, D. A.; Brooks, C. L. Performance Comparison of the Generalized Born and Poisson Methods in the Calculation of the Electrostatic Solvation Energies for Protein Structures. *J. Comput. Chem.* **2004**, *25*, 265−284.
(64) Mongan, J.; Simmerling, C.; McCammon, A. J.; Case, D. A.; Onufriev, A. Generalized Born With a Simple, Robust Molecular Volume Correction. *J. Chem. Theory Comput.* **2007**, *3*, 156−169.
(65) Scott, W. R. P.; Hünenberger, P. H.; Tironi, I. G.; Mark, A. E.; Billeter, S. R.; Fennen, J.; Torda, A. E.; Huber, T.; Krüger, P.; van Gunsteren, W. F. The GROMOS Biomolecular Simulation Program Package. *J. Phys. Chem. A* **1999**, *103*, 3596−3607.

DOI: 10.1021/acs.langmuir.5b03170
Langmuir XXXX, XXX, XXX−XXX